PEDOT Encapsulated FeOF Nanorod Cathodes for High Energy Lithium-Ion Batteries

Xiulin Fan,[†] Chao Luo,[†] Julia Lamb,[†] Yujie Zhu,[†] Kang Xu,[§] and Chunsheng Wang*,[†]

[†]Department of Chemical and Biomolecular Engineering, University of Maryland, College Park, Maryland 20742, United States
[§]Electrochemistry Branch, Power and Energy Division Sensor and Electron Devices Directorate, U.S. Army Research Laboratory, Adelphi, Maryland 20783, United States

S *Supporting Information*

ABSTRACT: Conversion-reaction cathodes can potentially double the energy density of current Li-ion batteries. However, the poor cycling stability, low energy efficiency, and low power density of conversion-reaction cathodes limit their applications for Li-ion batteries. Herein, we report a revolutionary advance in a conversion-reaction cathode by developing a core−shell FeOF@PEDOT nanorods, in which partial substitution of fluorine with oxygen in FeF_3 substantially enhance the reaction kinetics and reduce the potential hysteresis, while conformal nanolayer PEDOT coating provides a roubst fast electronic connection and prevents the side reactions. The FeOF@PEDOT nanorods deliver a capacity of 560 mA h g^{-1} at 10 mA g^{-1} with an energy density of >1100 W h kg^{-1}, which is more than two times higher than the theoretical energy density of $LiCoO_2$. The FeOF@PEDOT nanorods can maintain a capacity of ∼430 mA h g^{-1} at 50 mA g^{-1} (840 W h kg^{-1}) for over 150 cycles with capacity decay rate of only 0.04% per cycle, which is 2 orders of magnitude lower than the capacity decay rate ever reported among all conversion-reaction cathodes. Detailed characterizations were conducted to identify the structure and mechanism responsible for these significant improvements that could translate into a Li-ion cell with a 2× increase in energy density.

KEYWORDS: *Cathode material, conversion reaction, FeOF, PEDOT*
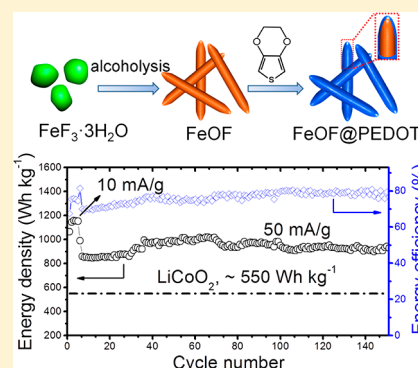
N owadays, intercalation compound cathodes have been widely used in commercial lithium-ion batteries (LIBs) due to the long cycle life and the high energy efficiency. However, the nature of only transferring 0.5−1.0 electrons per formula unit during charge/discharge limits the specific capacity of the materials, largely restricting their applications for electric vehicles.[1−3] Since the energy density of commercial Li-ion batteries is controlled by intercalation compound cathodes, the high energy cathode materials with low cost are urgently needed for electric vehicle batteries.[4−6] The fluoride[7−12] and sulfide[13−17] conversion cathodes can deliver over three times higher capacity than conventional intercalation cathodes, which are very promising candidates to replace the current intercalation cathodes.[13,14,18] The conversion cathode M_aX_b (M = Fe, Co, Ni, Cu etc., X = S, F) are capable of accommodating more than one Li^+ per transition metal core in their reaction with Li:

$$MX_n + nLi^+ + ne \rightleftharpoons nLiX + M \tag{1}$$
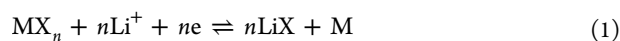
M = Fe, Ni, Co, Cu; X = $1/2S^{2-}$ or F^-, and n = 2 or 3.

Among these conversion chemistries, the FeF_3 shows a high lithiation/delithiation potential due to the higher ionicity of F^-, providing a highest energy density.[8,19] However, the pure FeF_3 exhibits slow reaction kinetics and large potential hysteresis during the lithiation/delithiation due to the poor diffusivity of ions, slow conversion reaction, and the low conductivity of fluorides induced by the strong ionic bond between Fe and fluorine.[9,20−23]

Amatucci et al.[23−25] utilized oxygen to partially substitute fluorine in iron fluoride to reduce ionicity between Fe^{3+} and F^-, which increased the lattice defects, thus reducing the potential hysteresis and overpotential of the iron fluorides. The FeO_xF_{2-x} cathode materials also show higher average lithiation/delithaition potentials, more symmetry lithiation/delithiation curves, and better cycling stability than the unsubstituted iron fluorides.[23,24] It is reported that the enhancement of defects of Fe atomic lattices and reduction of the ionicity through oxygen substitution can also restrict the overgrowth of Fe nanoparticles[26] and improve the electronic conductivity of the metal fluoride.[8] Moreover, FeOF also has higher theoretical specific capacity (885 mA h g^{-1}) than pure fluoride (712 mA h g^{-1} for FeF_3 and 571 mA h g^{-1} for FeF_2). These combined advantages of $FeOF_x$ render it a promising cathode material for high energy density Li-ion batteries. Although extensive efforts have been conducted on $FeOF_x$ cathode materials,[23,24,26−33] $FeOF_x$ still shows poor rate capability and cycling stability and lower Coulombic efficiency[24,32] due to the low electronic conductivity and ion diffusion coefficient of $FeOF_x$, the side reaction of

lithitation formed nano-Fe with electrolyte,[34] the agglomeration of these nano Fe nanoparticles,[34−36] and the complexity of the conversion reaction mechanism.[23]

In this study, we synthesized a nanolayer of conducting polymer of poly(3,4-ethylenedioxythiophene) (PEDOT) coated FeOF nanorod to enhance the reaction kinetics and to prevent the side reaction of Fe with electrolytes. The FeOF@PEDOT nanorods delivered a high capacity of 560 mA h g^{-1} with an extremely high energy density of >1100 W h kg^{-1} at 10 mA g^{-1} and maintained a high capacity of ~430 mA h g^{-1} (840 W h kg^{-1}) at 50 mA g^{-1} for over 150 cycles with capacity decay rate of 0.04% per cycle, which is 2 orders of magnitude lower than capacity decay rate ever reported among all FeF$_3$, and FeOF$_x$ cathodes at similar capacity levels. The two times higher energy density than commercial LiCoO$_2$ and low capacity decay rate each cycle make the FeOF@PEDOT nanorods are promising cathodes for next generation high energy Li-ion batteries.

Overall strategy for synthesis of FeOF@PEDOT is schematically depicted in Figure 1. A detailed description is given in the
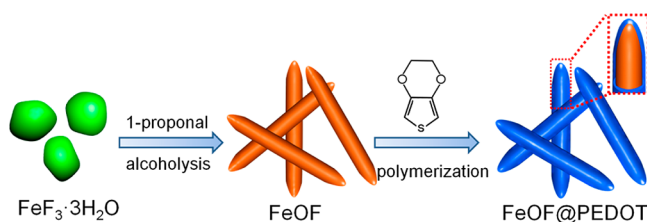
Figure 1. Schematic illustration for the synthesis of FeOF@PEDOT core−shell nanorods.

experimental section. Briefly, FeOF nanorods were first prepared by solvent-thermal treatment of FeF$_3$·3H$_2$O in 1-proponal solution at 210 °C. During the solvent-thermal synthesis, the FeF$_3$·3H$_2$O was reconstructed in the presence of 1-proponal and resulted in the formation of FeOF.[31] Then, in the presence of oxidizer, the 3,4-ethylenedioxythiophene (EDOT) was in situ polymerized into PEDOT, which uniformly coated on the surface of the FeOF. PEDOT was one of the most used conducting polymers in the past few decades due to its high conductivity, good thermal and environmental stability, and simple synthesis.[37−40] Compared to the classical carbon coating, the in situ PEDOT coating does not require high temperature and can therefore avoid the possible reduction of Fe^{3+} as well as ensure the structural stability for the FeOF nanorods, which is essential for this conversion cathode material. The core−shell structured FeOF@PEDOT nanorods are expected to simultaneously resolve the aforementioned challenges of FeOF cathodes by combining the FeOF nanorod architecture and the conformal polymeric coating of PEDOT. The nanorods with ~100 nm in diameter and ~800 nm length can dramatically reduce the diffusion distance of ions during the charge and discharge, thereby improving the kinetics of the lithiation/delithiation. The homogeneous conformal coating of conductive polymer provides a continuous and fast electronic path in the electrode, which allows faster charge transport.[39−42] Moreover, PEDOT conformal coating could avoid the nanoparticle aggregation upon cycling, maintain the structural stability against volume variation, and prevent the side reactions between the in situ formed nano-Fe^0 species and electrolyte during cycling,[34] which would benefit the cycling stability.

The crystal structure and the detailed morphology of the as-synthesized materials were characterized by X-ray diffraction (XRD), scanning electron microscopy (SEM) and transmission electron microscopy (TEM) analysis. Figure 2 shows the XRD
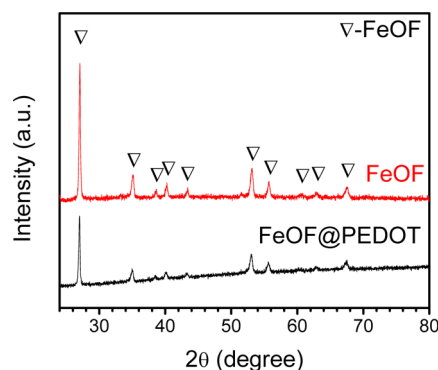

**Figure 2.** XRD patterns for the as-synthesized FeOF and FeOF@PEDOT.

patterns for the FeOF and FeOF@PEDOT. It was found that all the diffraction peaks can be well-indexed to FeOF (JCPDS 18-0648) with the tetragonal structure in space group $P4_2/mnm$. After coating with conducting polymer PEDOT, no new peaks are observed, indicating that the in situ polymerized PEDOT is in the amorphous state. This is consistent with the previous polymerization of EDOT.[38,39]

After PEDOT coating, the color of FeOF powders changed from yellow to dark brown (Figure S1). Figure 3 compares the morphology and structure of FeOF before and after PEDOT coating. Figure 3a and b shows the scanning electron microscopy (SEM) images of pure FeOF nanorods at different magnifications. These FeOF particles exhibit nanorod morphology with size of about 800 nm × 100 nm. The regular crystallographic faces in the high magnification SEM image (Figure 3b) indicate well-crystallized particles. High resolution transmission electron microscopy (HRTEM) and fast Fourier transform (FFT) of the nanorods in Figure 3c reveal lattice fringes with a spacing of 0.25 nm which corresponds to the (101) planes of FeOF (tetragonal, $P4_2/mnm$). HRTEM image and corresponding FFT image for larger area are shown in Figure S2. The distinct lattice fringes and the FFT dots clearly show that the nanorods are in single crystallinity. Figure 3d and e depict the SEM images of PEDOT coated FeOF nanparticles. As expected, nanorod features are perfectly preserved with a uniform layer for the FeOF@PEDOT during the polymerization of EDOT, while the surface becomes rather blurry, indicating the successful coating of PEDOT. The core−shell feature can further be elucidated from the representative HRTEM image that there is a notable contrast between the FeOF nanorods and PEDOT shells, as shown in Figure 3f. The outer layers (~12 nm) are like sheaths, which completely encapsulate the crystalline FeOF nanorods (Figure 3f). To verify that the surface layer on the FeOF is PEDOT, we conducted elemental mapping by means of energy-dispersive X-ray spectroscopy (EDS), as shown in Figure S3. Uniform S distribution in the material proves that all of the FeOF nanorods are covered by the sulfur-rich PEDOT layers.

The PEDOT coating on the FeOF was further identified by Fourier transform infrared (FTIR) and Raman spectroscopy. The results are shown in Figure 4. The formation of PEDOT is confirmed by the C═C ring and C−O−R bond vibrations at
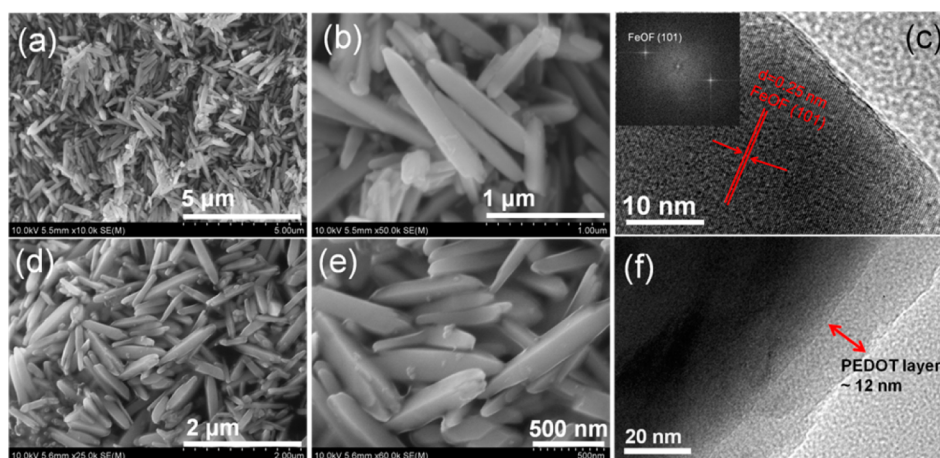
Figure 3. (a and b) SEM images of the as-synthesized FeOF nanorods; (c) HRTEM image of the as-synthesized FeOF nanorods; (d and e) SEM images of the PEDOT coated FeOF nanorods; (f) TEM image of the PEDOT coated FeOF nanorods. The inset of panel c is the corresponding FFT patterns.
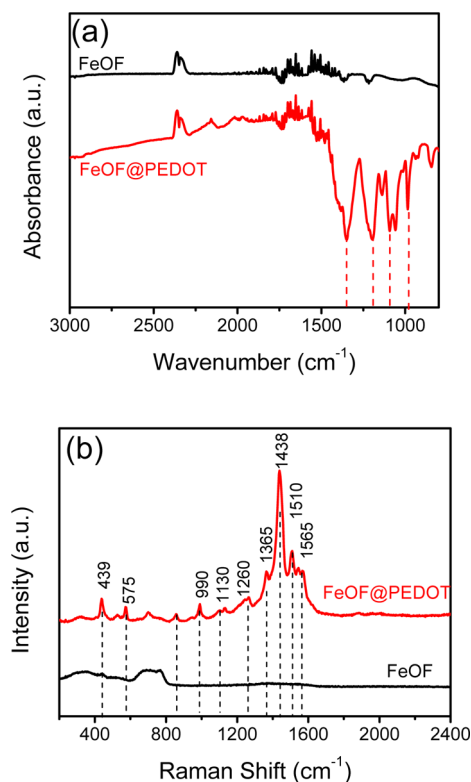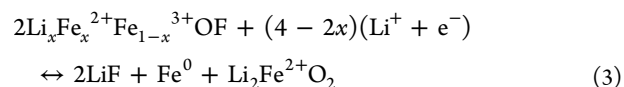

Figure 4. FTIR (a) and Raman (b) spectra for FeOF (black line) and FeOF@PEDOT (red line). All of the labeled peaks for the FeOF@PEDOT can be indexed to PEDOT bands.

$\sim$1180 cm^{-1} and the C–S vibration at 929 cm^{-1} in the FTIR spectra. The polymer p-doping is also indicated by the bands at 1320 cm^{-1}. These vibration features are in line with the polymerized PEDOT materials,[40,43] which confirm the formation of PEDOT on the surface of the FeOF nanorods. The Raman spectra of as-prepared FeOF@PEDOT and FeOF are shown in Figure 4b. All of the observed bands are attributable to PEDOT.[37] The strong band at 1438 cm^{-1} is assigned to the stretching vibration of C=C ring arising from neutral parts existing between localized elementary excitations such as positive polarons or bipolarons generated upon doping during synthesis.[44] The upward shift for this peak compared

with the standard peak of PEDOT indicates good oxidation (doping),[37] which enhances the favorable conductivity for the polymer. The unique hierarchical nanorod core/sell structure where the inner nanorods can effectively suppress the pulverization, while the outer PEDOT can enhance electrode stability, and avoid the dissolution and reaction of Fe ions to electrolytes. The amount of PEDOT coating in FeOF@ PEDOT was determined based on the weight loss of the FeOF@PEDOT after rinsing in nitrite acid to remove the inner FeOF. The FeOF@PEDOT was treated with nitrite acid solution after breaking the PEDOT shell using high power ultrasonication. During the treatment, the FeOF dissolved into the acid, as shown in Figure S4. The mass ratio of PEDOT in the composite is ca. 12 wt %.

The electrochemical performance of the FeOF@PEDOT was investigated using cyclic voltammetry (CV) and galvanostatic charge/discharge cycling. Figure 5a shows the first four CV curves of a FeOF@PEDOT composite cathode in the voltage range of 4.0−1.2 V at a scanning rate of 0.1 mV/s. In the first lithiation, two reduction peaks at approximate 2.4 and 1.2 V can be observed, which correspond to the intercalation (eq 2) and conversion reaction (eq 3) of FeOF as expressed below:[25,33]

$$Fe^{3+}OF + xLi^+ + xe^- \leftrightarrow Li_xFe_x^{2+}Fe_{1-x}^{3+}OF \tag{2}$$

$$2Li_xFe_x^{2+}Fe_{1-x}^{3+}OF + (4-2x)(Li^+ + e^-)$$
$$\leftrightarrow 2LiF + Fe^0 + Li_2Fe^{2+}O_2 \tag{3}$$

In the following cycles, the potentials of these two reactions shift up (2.4 V → 2.8 V; and 1.2 V → 1.9 V) due to relaxation of stress/strain during the first cycle. In the anodic scan process, these reactions overlap, only a large delithiation peak at $\sim$2.7 V with a very small shoulder at 3.15 V is observed. The shoulder can be ascribed to the intercalation reaction (eq 2), while a large peak at 2.7 V is attributed to conversion reaction (eq 3). The potential hysteresis at a scan rate of 0.1 mV s^{-1} is 0.35 V for intercalation reaction and 0.8 V for conversion reaction, which is smaller than reported FeOF and FeF$_3$ at similar scan rate.[9,24] The overlaps of the CV profiles in the following cycles indicate the excellent reversibility for the FeOF@PEDOT electrode during lithiation/delithiation cycles. Figure 5b shows the voltage profile of FeOF@PEDOT electrode at a current
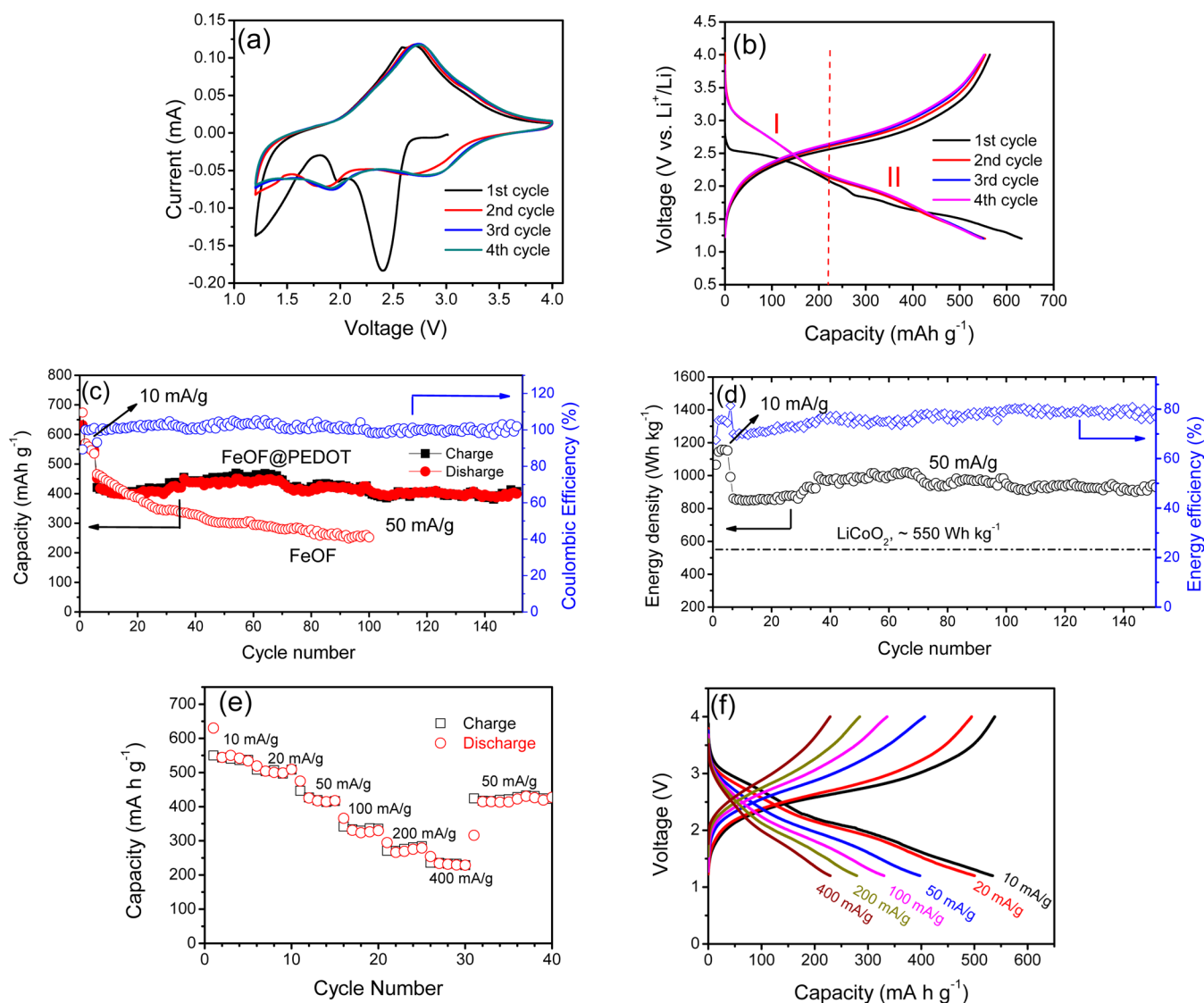
Figure 5. Electrochemical performance of the FeOF and FeOF@PEDOT: (a) CV curves for the FeOF@PEDOT at a scanning rate of 0.1 mV s^{-1} in the voltage range of 1.2−4.0 V; (b) electrochemical charge/discharge curves of as-synthesized FeOF@PEDOT composite at a constant current of 10 mA g^{-1} in the voltage window 1.2−4.0 V at room temperature; (c) cycling performance of FeOF@PEDOT composite; (d) discharge energy density vs cycle number shown along with the theoretical discharge energy density of LiCoO$_2$ cathode material (550 W h kg^{-1} based on the mass of LiCoO$_2$ only); (e) rate capability at different current rates; (f) voltage−capacity curves at different rates (increased from 10 mA g^{-1} to 400 mA g^{-1}).

density of 10 mA g^{-1} between 4.0 and 1.2 V. The initial discharge and charge capacities of FeOF@PEDOT electrode are 630 mA h g^{-1} and 564 mA h g^{-1}, respectively, exhibiting a recorded high Coulombic efficiency of 89% for conversion cathode systems. The discharge curves can be divided into two plateaus (Regions I and II as denoted in the Figure 5b), which is in good agreement with the two peaks in the CV curves. As demonstrated in CV, the average potential plateau in regions I and II shift up in the second lithiation and remain stable in the following lithiations. In Region I, the potential plateau ranging from 3.25 V to ∼2.25 V, corresponding to the intercalation reaction of Li$^+$ into the lattice of FeOF crystallite (eq 2),[30] delivers a capacity of ∼220 mA h g^{-1}. After the intercalation reaction, conversion reaction (eq 3) takes place, giving additional capacity of ∼330 mA h g^{-1} in the potential range of 2.25−1.2 V. These two discharge plateaus have much higher potentails than those of the two lithiation plateaus in the FeS$_2$ system,[13−16] rendering the energy storage density much higher for the FeOF system. The delithiation profile of FeOF@

PEDOT electrode only shows single slop plateau due to the overlap of the intercalation with conversion reaction as demonstrated in CV. In the meantime, the hysteresis between charge and discharge profiles is much smaller than that of FeF$_3$ systems,[7,45,46] indicating the sufficiently improved kinetics for the FeOF@PEDOT system. These properties guarantee the present FeOF@PEDOT as one of the most promising conversion cathode materials for LIBs.

The effect of PEDOT coating on the cycling stability and Coulombic efficiency of FeOF@PEDOT was investigated. Figure 5c shows the cycling stability and Coulombic efficiency of the FeOF@PEDOT and FeOF electrodes. Both of the electrodes were precycled between 1.2 and 4 V at a current rate of 10 mA g^{-1} for 5 cycles to fully activate the cathode materials. Then the current density was increased to 50 mA g^{-1} in the following cycles to investigate the long cycling stability. Both FeOF and FeOF@PEDOT showed a high capacity of ∼550 mA h g^{-1} at 10 mA g^{-1}. The FeOF@PEDOT cathode showed a very stable cycling performance after 5 cycle activation at a low
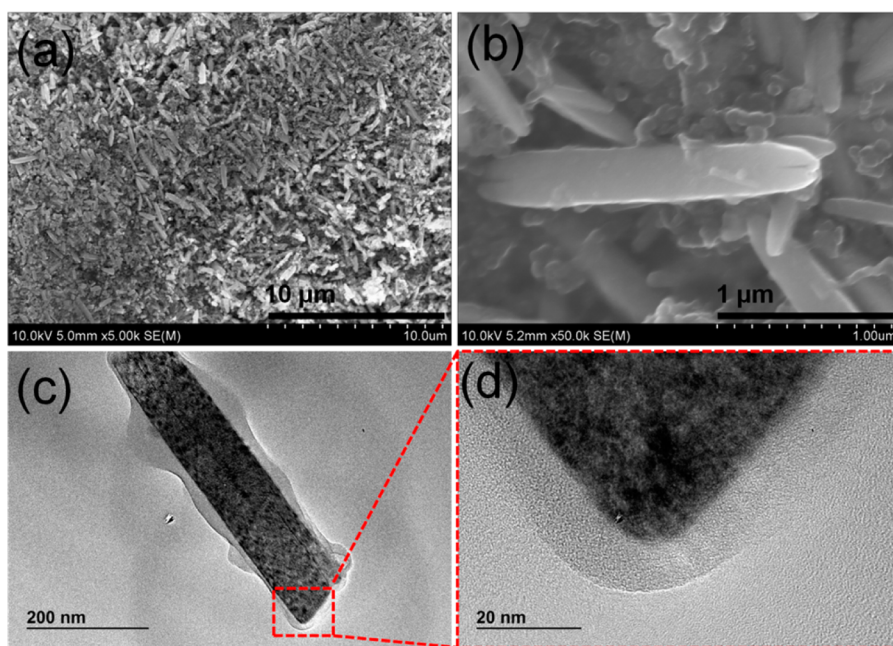
Figure 6. Different magnification SEM (a, b) and TEM (c, d) images for the FeOF@PEDOT electrode charged to 4 V after 20 cycles. SEM and TEM images show that the FeOF@PEDOT after cycling kept the same morphology as the pristine synthesized FeOF@PEDOT. HRTEM shows that the crystal of FeOF breaks into nanodomains with size of less than 10 nm, which are encapsulated by the PEDOT.

current. The discharge capacity remained at the very high value of ∼407 mA h g^{-1} even after 150 cycles with a capacity retention of over 94% (0.04% decay per cycle) and high average Coulombic efficiency near to 100% (Figure 5c). In contrast, the bare FeOF nanorod electrode only delivered a capacity of ∼260 mA h g^{-1} after 100 cycles, a discharge capacity retention value of only 55% of the capacity at sixth cycle. A slightly lower efficiency was observed for the FeOF nanorods due to the partial reaction between electrolyte and in situ formed Fe nanoparticles (Figure S5). A small capacity of less than 50 mA h g^{-1} was contributed from PEDOT polymer itself in the potential range of 4.0−1.2 V (Figure S6), in line with prior investigations.[40] Considering that the PEDOT mass only accounts for 12 wt % in the composite, the capacity provided by PEDOT should be less than 2% and considered negligible. The capacity of the FeOF@PEDOT cathode is much larger than that (140 mA h g^{-1}) of the conventional LiCoO$_2$ intercalation cathode materials. This enables the present FeOF@PEDOT cathode to have a much higher discharge energy density than the theoretical energy density of a LiCoO$_2$ cathode (Figure 5d) in spite of its lower voltage. As shown in Figure 5d, the present FeOF@PEDOT composite cathode materials delivered a stable discharge energy density over 840 W h kg^{-1} during the entire 150 cycles, which is much higher than the theoretical energy density of conventional LiCoO$_2$ (∼550 W h kg^{-1}). At a low current of 10 mA g^{-1}, FeOF@PEDOT can even deliver 1100 W h kg^{-1} (as shown for the first 5 cycles in Figure 5d), which is two times larger than the theoretical energy density (can only be obtained at an extreme low current) of LiCoO$_2$. Table S1 summarized electrochemical cycling performance of all reported Fe-based conversion cathode materials. The FeOF@PEDOT shows the longest cycling numbers, 2 orders of magnitude lower capacity decay per cycle, highest energy density among all Fe-based conversion-reaction cathodes cycled in the similar potential ranges. To the best of our knowledge, such a good cycling

performance with such high discharge energy density based on a reversible conversion reaction at room temperature has not been reported before.[13,14,47,48]

In addition to the superior cycling performance, the FeOF@PEDOT electrode also exhibits an impressive rate performance. Figure 5e presents the rate capability of the FeOF@PEDOT composite with the corresponding charge−discharge curves plotted in Figure 5f. As the current rate increased from 10 mA g^{-1}, 50 mA g^{-1} to 400 mA g^{-1}, the discharge capacity only decreased from 550 to 420 and 230 mAh g^{-1}, respectively, indicating high rate capability of the FeOF@PEDOT cathode materials. The FeOF@PEDOT shows the best rate performances among all the Fe-based fluoride conversion reaction cathodes reported to date. Moreover, when the current density is finally returned to the value of 50 mA g^{-1}, the capacity of 420 mA h g^{-1} is completely recovered, implying the excellent tolerance for the rapid lithium ion insertion/extraction cycles. The FeOF@PEDOT cathodes are promising cathode material for next-generation of high energy low cost Li-ion batteries.

The morphology and the composition of the FeOF@PEDOT after cycling were characterized using SEM, TEM, HRTEM, and SAED techniques. Figure 6a,b and Figure S7 show the morphology of FeOF@PEDOT after the 20th charge/discharge cycle. The original morphology of the FeOF@PEDOT nanorods is well-preserved. The detailed TEM and HRTEM images in Figure 6c,d and Figure S8 show that the single crystal of FeOF core covered by PEDOT has converted into plenty of tiny nanodomains after 20 cycles. The conducting polymer still conformally coated on the FeOF surface, effectively protecting the inner FeOF from reaction with electrolyte and maintaining the high electronic conductivity.[15] In contrast, the bare FeOF nanorod electrode showed large amount of creaks, cavities in FeOF nanorods (Figure S9). As shown in Figure S9, some FeOF nanorods are even pulverized into nanoparticles. The loss of the electroactive FeOF species during charge/discharge cycles resulted in the

continuoues capacity decay. Moreover, the pulverization during lithiation and delithiation accelerated the side reaction of in situ formed Fe with electrolyte[34] and increased the contact resistance, resulting in poor electrochemical performance and the structure decay for the bare FeOF nanorods.

The extremely superior electrochemical performance and structure stability of FeOF@PEDOT nanorod electrode can probably be attributed to the distinct nanorod morphology of the FeOF and more importantly to a synergetic activity of PEDOT coating that offers the following benefits: First, the uniform nanoscale one-dimensional FeOF cathode affords a shorter Li^+ and electron transport pathway, enhancing conversion reaction kinetics and utilization of the active material upon discharge and charge. Second, the conformal thin PEDOT coating on the surface of the FeOF nanorods not only remarkably improve the effective electrical conductivity of the composite, but also provide continuous conductive paths between FeOF nanorods, and therefore reduce the particle to particle interfacial resistance. Third, the thin PEDOT shells can protect the inner FeOF nanorod cores from directly contacting with the electrolyte and alleviate the side reactions at the interface between the in situ formed Fe^0 nanoparticles and the electrolyte, resulting in the structural and interfacial stability of FeOF nanorods. This feature is especially important for the TM fluorides, since the reaction between the TM and the electrolyte usually causes the fast decay of the reversibility.[34,49,50] Fourthly, the PEDOT layers with favorable mechanical flexibility can efficiently inhibit the aggregation of the FeOF nanorods and preserve the structural integrity of the electrode. The above synergetic effect ensures the large capacity as well as superior cycling performance of the PEDOT coated FeOF nanorods.

In summary, FeOF@PEDOT core−shell nanorod cathode material for the LIBs was successfully fabricated by a facile and scalable synthesis method. Benefiting from the nanorod morphology of FeOF and conductive pretecting PEDOT coating layer, FeOF@PEDOT nanorod composites provide an extremely high discharge energy density of 1100 W h kg^{-1} at 10 mA g^{-1} at room temperature, which is two times higher than theoretical energy density of $LiCoO_2$. FeOF@PEDOT nanorod can maintain a discharge energy density of 840 W h kg^{-1} at 50 mA g^{-1} for 150 cycles with energy density decay of only 0.04% per cycle. Meanwhile, the as-fabricated FeOF@PEDOT core−shell electrode also shows a high rate capability and high energy efficiency of about 80%. The FeOF@PEDOT shows the best overall electrochemical performance among all Fe-based conversion cathodes reported. The FeOF nanorod with PEDOT coating cathodes could open up a novel avenue for the practical application of conversion reaction cathode materials for LIBs.

■ ASSOCIATED CONTENT

Ⓢ Supporting Information

The Supporting Information is available free of charge on the ACS Publications website at DOI: 10.1021/acs.nanolett.5b03601.

Details of the synthesis, characterization, electrochemical measurements, additional figures (Figure S1−S9), additional table (Table S1) (PDF)

■ AUTHOR INFORMATION

Corresponding Author

*E-mail: cswang@umd.edu.

Notes

The authors declare no competing financial interest.

■ REFERENCES

(1) Whittingham, M. S. *Chem. Rev.* **2014**, *114*, 11414−11443.

(2) Ma, R.; Dong, Y.; Xi, L.; Yang, S.; Lu, Z.; Chung, C. *ACS Appl. Mater. Interfaces* **2013**, *5*, 892−897.

(3) Goodenough, J. B.; Kim, Y. *Chem. Mater.* **2010**, *22*, 587−603.

(4) Andre, D.; Kim, S.-J.; Lamp, P.; Lux, S. F.; Maglia, F.; Paschos, O.; Stiaszny, B. *J. Mater. Chem. A* **2015**, *3*, 6709−6732.

(5) Xu, B.; Qian, D.; Wang, Z.; Meng, Y. S. *Mater. Sci. Eng., R* **2012**, *73*, 51−65.

(6) Etacheri, V.; Marom, R.; Elazari, R.; Salitra, G.; Aurbach, D. *Energy Environ. Sci.* **2011**, *4*, 3243−3262.

(7) Reddy, M. A.; Breitung, B.; Chakravadhanula, V. S. K.; Wall, C.; Engel, M.; Kübel, C.; Powell, A. K.; Hahn, H.; Fichtner, M. *Adv. Energy Mater.* **2013**, *3*, 308−313.

(8) Amatucci, G. G.; Pereira, N. *J. Fluorine Chem.* **2007**, *128*, 243−262.

(9) Liu, P.; Vajo, J. J.; Wang, J. S.; Li, W.; Liu, J. *J. Phys. Chem. C* **2012**, *116*, 6467−6473.

(10) Gu, W.; Magasinski, A.; Zdyrko, B.; Yushin, G. *Adv. Energy Mater.* **2015**, *5*, 10.1002/aenm.201401148.

(11) Li, C.; Mu, X.; van Aken, P. A.; Maier, J. *Adv. Energy Mater.* **2013**, *3*, 113−119.

(12) Li, H.; Richter, G.; Maier, J. *Adv. Mater.* **2003**, *15*, 736−739.

(13) Liu, J.; Wen, Y.; Wang, Y.; van Aken, P. A.; Maier, J.; Yu, Y. *Adv. Mater.* **2014**, *26*, 6025−6030.

(14) Evans, T.; Piper, D. M.; Kim, S. C.; Han, S. S.; Bhat, V.; Oh, K. H.; Lee, S.-H. *Adv. Mater.* **2014**, *26*, 7386−7392.

(15) Son, S.-B.; Yersak, T. A.; Piper, D. M.; Kim, S. C.; Kang, C. S.; Cho, J. S.; Suh, S.-S.; Kim, Y.-U.; Oh, K. H.; Lee, S.-H. *Adv. Energy Mater.* **2014**, *4*, 10.1002/aenm.201300961.

(16) Zhang, D.; Wang, X. L.; Mai, Y. J.; Xia, X. H.; Gu, C. D.; Tu, J. P. *J. Appl. Electrochem.* **2012**, *42*, 263−269.

(17) Zhang, S. S. *J. Mater. Chem. A* **2015**, *3*, 7689−7694.

(18) Rui, X.; Tan, H.; Yan, Q. *Nanoscale* **2014**, *6*, 9889−9924.

(19) Li, H.; Balaya, P.; Maier, J. *J. Electrochem. Soc.* **2004**, *151*, A1878−A1885.

(20) Arai, H.; Okada, S.; Sakurai, Y.; Yamaki, J.-i. *J. Power Sources* **1997**, *68*, 716−719.

(21) Wang, F.; Robert, R.; Chernova, N. A.; Pereira, N.; Omenya, F.; Badway, F.; Hua, X.; Ruotolo, M.; Zhang, R.; Wu, L.; Volkov, V.; Su, D.; Key, B.; Whittingham, M. S.; Grey, C. P.; Amatucci, G. G.; Zhu, Y.; Graetz, J. *J. Am. Chem. Soc.* **2011**, *133*, 18828−18836.

(22) Doe, R. E.; Persson, K. A.; Meng, Y. S.; Ceder, G. *Chem. Mater.* **2008**, *20*, 5274−5283.

(23) Ko, J. K.; Wiaderek, K. M.; Pereira, N.; Kinnibrugh, T. L.; Kim, J. R.; Chupas, P. J.; Chapman, K. W.; Amatucci, G. G. *ACS Appl. Mater. Interfaces* **2014**, *6*, 10858−10869.

(24) Pereira, N.; Badway, F.; Wartelsky, M.; Gunn, S.; Amatucci, G. G. *J. Electrochem. Soc.* **2009**, *156*, A407−A416.

(25) Cosandey, F.; Su, D.; Sina, M.; Pereira, N.; Amatucci, G. G. *Micron* **2012**, *43*, 22−29.

(26) Wiaderek, K. M.; Borkiewicz, O. J.; Pereira, N.; Ilavsky, J.; Amatucci, G. G.; Chupas, P. J.; Chapman, K. W. *J. Am. Chem. Soc.* **2014**, *136*, 6211−6214.

(27) Chevrier, V. L.; Hautier, G.; Ong, S. P.; Doe, R. E.; Ceder, G. *Phys. Rev. B: Condens. Matter Mater. Phys.* **2013**, *87*, 094118.

(28) Sina, M.; Nam, K. W.; Su, D.; Pereira, N.; Yang, X. Q.; Amatucci, G. G.; Cosandey, F. *J. Mater. Chem. A* **2013**, *1*, 11629−11640.

(29) Gocheva, I. D.; Tanaka, I.; Doi, T.; Okada, S.; Yamaki, J.-i. *Electrochem. Commun.* **2009**, *11*, 1583−1585.

(30) Zhou, Y.-N.; Sina, M.; Pereira, N.; Yu, X.; Amatucci, G. G.; Yang, X.-Q.; Cosandey, F.; Nam, K.-W. *Adv. Funct. Mater.* **2015**, *25*, 696−703.

(31) Zhu, J.; Deng, D. *Angew. Chem., Int. Ed.* **2015**, *54*, 3079−3083.

(32) Kitajou, A.; Komatsu, H.; Nagano, R.; Okada, S. *J. Power Sources* **2013**, *243*, 494−498.

(33) Wiaderek, K. M.; Borkiewicz, O. J.; Castillo-Martínez, E.; Robert, R.; Pereira, N.; Amatucci, G. G.; Grey, C. P.; Chupas, P. J.; Chapman, K. W. *J. Am. Chem. Soc.* **2013**, *135*, 4070−4078.

(34) Sina, M.; Thorpe, R.; Rangan, S.; Pereira, N.; Bartynski, R. A.; Amatucci, G. G.; Cosandey, F. *J. Phys. Chem. C* **2015**, *119*, 9762−9773.

(35) Yersak, T. A.; Macpherson, H. A.; Kim, S. C.; Le, V.-D.; Kang, C. S.; Son, S.-B.; Kim, Y.-H.; Trevey, J. E.; Oh, K. H.; Stoldt, C.; Lee, S.-H. *Adv. Energy Mater.* **2013**, *3*, 120−127.

(36) Takada, K.; Kitami, Y.; Inada, T.; Kajiyama, A.; Kouguchi, M.; Kondo, S.; Watanabe, M.; Tabuchi, M. *J. Electrochem. Soc.* **2001**, *148*, A1085−A1090.

(37) Sakamoto, S.; Okumura, M.; Zhao, Z.; Furukawa, Y. *Chem. Phys. Lett.* **2005**, *412*, 395−398.

(38) Kim, J.; Yoo, J.-K.; Jung, Y. S.; Kang, K. *Adv. Energy Mater.* **2013**, *3*, 1004−1007.

(39) Zeng, Y.; Han, Y.; Zhao, Y.; Zeng, Y.; Yu, M.; Liu, Y.; Tang, H.; Tong, Y.; Lu, X. *Adv. Energy Mater.* **2015**, *5*, 10.1002/aenm.201402176.

(40) Ma, D.-l.; Cao, Z.-y.; Wang, H.-g.; Huang, X.-l.; Wang, L.-m.; Zhang, X.-b. *Energy Environ. Sci.* **2012**, *5*, 8538−8542.

(41) Zhao, L.; Hu, Y.-S.; Li, H.; Wang, Z.; Chen, L. *Adv. Mater.* **2011**, *23*, 1385−1388.

(42) Guo, L.; Zhang, Y.; Wang, J.; Ma, L.; Ma, S.; Zhang, Y.; Wang, E.; Bi, Y.; Wang, D.; McKee, W. C.; Xu, Y.; Chen, J.; Zhang, Q.; Nan, C.; Gu, L.; Bruce, P. G.; Peng, Z. *Nat. Commun.* **2015**, *6*, 10.1038/ncomms8898.

(43) Lepage, D.; Michot, C.; Liang, G.; Gauthier, M.; Schougaard, S. B. *Angew. Chem., Int. Ed.* **2011**, *50*, 6884−6887.

(44) Furukawa, Y. *J. Phys. Chem.* **1996**, *100*, 15644−15653.

(45) Ma, R.; Wang, M.; Tao, P.; Wang, Y.; Cao, C.; Shan, G.; Yang, S.; Xi, L.; Chung, J. C. Y.; Lu, Z. *J. Mater. Chem. A* **2013**, *1*, 15060−15067.

(46) Armstrong, M. J.; Panneerselvam, A.; O'Regan, C.; Morris, M. A.; Holmes, J. D. *J. Mater. Chem. A* **2013**, *1*, 10667−10676.

(47) Cabana, J.; Monconduit, L.; Larcher, D.; Palacín, M. R. *Adv. Mater.* **2010**, *22*, E170−E192.

(48) Li, L.; Meng, F.; Jin, S. *Nano Lett.* **2012**, *12*, 6030−6037.

(49) Hua, X.; Robert, R.; Du, L.-S.; Wiaderek, K. M.; Leskes, M.; Chapman, K. W.; Chupas, P. J.; Grey, C. P. *J. Phys. Chem. C* **2014**, *118*, 15169−15184.

(50) Wang, F.; Kim, S.-W.; Seo, D.-H.; Kang, K.; Wang, L.; Su, D.; Vajo, J. J.; Wang, J.; Graetz, J. *Nat. Commun.* **2015**, *6*, 10.1038/ncomms7668.